SECOND EUROPEAN CONFERENCE ON EARTHQUAKE ENGINEERING
AND SEISMOLOGY, ISTANBUL AUG. 25-29, 2014

FROM PLASTIC HINGE TO SHELL MODELS: RECOMMENDATIONS FOR RC WALL MODELS

Danilo TARQUINI[1], João ALMEIDA[2], Katrin BEYER[3]

ABSTRACT

The severe damage and collapse of many reinforced concrete (RC) wall buildings in the recent earthquakes of Chile (2010) and New Zealand (2011) have shown that RC walls did not perform as well as expected based on the design calculations required by the modern codes of both countries. In this context, it seems appropriate to intensify research efforts in more accurate simulations of damage indicators, in particular local engineering demand parameters such as material strains, which are central to the application of performance-based earthquake engineering. Potential modelling improvements will necessarily build on a thorough assessment of the limitations of current state-of-the-practice simulation approaches. This work aims to compare the response variability given by a spectrum of numerical tools commonly used by researchers and specialized practitioners, namely: plastic hinge analyses, distributed plasticity models, and detailed finite element simulations. It is shown that a multi-level assessment—wherein both the global and local levels are jointly investigated from the response analysis outcomes—is fundamental to define the dependability of the results. The latter is controlled by the attainment of material strain limits and the occurrence of numerical problems. Finally, the influence of shear deformations is analysed according to the same methodological framework.

INTRODUCTION

The idea that a structure should be able to resist minor seismic shaking without damage, withstand a moderate earthquake possibly experiencing some non-structural damage, and survive a major event without collapse, was clearly expressed in the late 1950s (SEAOC, 1959). Such statement embodies the concept of *performance-based earthquake engineering* (PBEE), which builds on the definition and the achievement of desired performance objectives (Bozorgnia & Bertero, 2004). The quantification of these targets evolved as scientifically validated knowledge built up, moving from empirical criteria (SEAOC, 1980) to equations founded upon physical principles and accounting for uncertainties (ATC-3-06, 1978). The advancement of PBEE induced the implementation of performance-based principles

[1] MSc student, UME School, Pavia, Italy. Visiting student at Earthquake Engineering and Structural Dynamics (EESD), School of Architectural, Civil and Environmental Engineering (ENAC), École Polytechnique Fédérale de Lausanne (EPFL), danilo.tarquini@epfl.ch
[2] Post-doctoral Researcher, Earthquake Engineering and Structural Dynamics (EESD), School of Architectural, Civil and Environmental Engineering (ENAC), École Polytechnique Fédérale de Lausanne (EPFL), joao.almeida@epfl.ch
[3] Assistant Professor, Earthquake Engineering and Structural Dynamics (EESD), School of Architectural, Civil and Environmental Engineering (ENAC), École Polytechnique Fédérale de Lausanne (EPFL), katrin.beyer@epfl.ch

in design codes (ASCE 7-02, 2002; EN1998-1, 2002), and especially in norms for the safety assessment of buildings (EN1998-3, 2005; FEMA, 2012).

All the above mentioned guidelines share a common feature: for each desired performance objective, they prescribe discrete, document-specific, performance levels—ranging from fully operational to collapse prevention—and discrete hazard levels. Although the latter are based on a probabilistic hazard analysis, the overall performance assessment is purely deterministic (regarding material properties and other member parameters, engineering computations, acceptance criteria, etc.). A central step for dependable performance assessment requires therefore the *definition of a set of engineering demand parameters* (EDPs) on which performance assessment can be based, and numerical simulation methods that are capable to accurately estimate them.

Until the mid-1990s, traditional EDPs were related to the global or member level, e.g. interstorey drift. However, the advancement of numerical simulation tools progressively spurred the supplementary use of local EDPs, i.e. quantities that refer to the material or sectional levels, which are considered to better and more directly correlate to damage (Berry et al., 2008). They include, amongst others, rebar strains, cover and core concrete strains, maximum curvature, and curvature ductility (Mackie & Stojadinovic, 2001). For instance, the reinforcing steel tensile strain can be defined as the EDP to assess the maximum residual crack width, which can then be compared to a reference value to assess if the damage level is negligible or requires a certain repair method. Other examples are the cover and core concrete compressive strains, which can be related to a certain degree of cover spalling.

It should stand clear from the above that, as PBEE pervades current design and seismic evaluation codes, a comprehensive structural (and non-structural) assessment should be based on an *accurate estimation of both global and local EDPs* (Berry et al., 2008). However, most of the comparisons typically focus on the global level of analysis and do not address comprehensively the relation between the latter and the local levels of the mathematical model in consideration.

The present work compares some of the most common modelling approaches for the simulation of the inelastic behaviour of RC walls based on a joint assessment of both global and local EDPs. Such an explicit multi-level study pinpoints the fundamental interplay between defined material strain limits, numerical problems, convergence issues, and the validity range of the results. The study also assesses if the prediction accuracy for global EDPs is similar to that of local EDPs, relating it to the adopted constitutive model and the finite element formulation (or the assumptions of the method, in the case of plastic hinge approaches).

In order to ease the interpretation of the results, a single RC wall is subjected to a simple pushover analysis, hence avoiding the number of additional complexities brought about by the use of nonlinear dynamic time histories or multi-member structural systems. Different shear span ratios are considered for the structural member, which is modelled according to the following techniques: plastic hinge analyses (PHAs), distributed plasticity models (DPMs), and detailed finite element (DFE) approaches. The selection was based on two criteria. First, it was intended to use simulation methods of distinct levels of complexity, roughly spanning the existing modelling spectrum. Second, only the approaches and software that are commonly used and available to researchers and specialized engineers were considered. The analysis of distinct shear span ratios is intended to evaluate the influence of shear deformations, which can be relevant for wall members.

It should be underlined that the purpose of this study is not to validate the results of different modelling approaches against experimental results, but rather to evaluate and interpret the scatter of the response provided by distinct state-of-practice simulation methods that build on the same (or as close as possible) input parameters, constitutive relations, confinement models, etc.

MULTI-LEVEL ANALYSES AND DEPENDABILITY

As stated in the previous section, the evaluation of global and local-level EDPs represents a central step in performance-based design or assessment of a structure. In order to accomplish this objective, a multi-level analysis is required, as well as a careful identification of the reliable part of the response. These two aspects are addressed in the following paragraphs.

Each modelling technique for the simulation of inelastic behaviour of structures is based on different background assumptions and distinct levels of analysis. Focusing on the models employed in

the present study (PHA, DPM and DFE), the inner level corresponds to the material constitutive relations. The next one in the hierarchy of analysis is the sectional level (herein considered as a local level as well), which is shared by both the PHAs and the DPMs. However, the former require a simplified approximation for the moment-curvature relation (in a bilinear form), whilst the latter take into account the complete sectional response, considering additionally the explicit interaction between the axial force and the bending moment(s). Finally, global levels are considered to include the element and the structural levels. Methods of PHA cannot assemble the response of multiple elements, and in that sense they do not present a structural level; such limitation is overcome with finite element formulations, either using beam-column (DPMs) or shell (DFEs) elements. Table 1 illustrates the different levels of analysis for PHAs, DPMs and DFE models.

Table 1. Levels of analysis in the employed modelling techniques.

Modelling technique	***Local Level***		***Global Level***	
	Material Level	**Sectional Level**	**Element Level**	**Structural Level**
PHA	✓	✓	✓	-
DPM	✓	✓	✓	✓
DFE	✓	-	✓	✓

The outcomes of each modelling approach should be carefully interpreted so that they can be effectively correlated to actual damage. The physically meaningful range of results—herein named dependable—is bounded by one of the following scenarios, whichever occurs at a lower value of drift: (i) a material strain limit, assumed as a threshold beyond which the defined constitutive relation is no longer representative of the true material behaviour; (ii) localization, a numerical problem inducing mesh-dependent results; and (iii) other numerical issues that render the output untrustworthy. These conditions can be expressed as:

$$Dependable\ Upper\ Bound = min\{Material\ Strain\ Limit, Localization, Numerical\ Issues\}$$

In this document, the material strain limit (MSL) is taken as the damage control limit state (DCLS) defined by Priestley et al. (2007). The corresponding concrete compression and steel tension strain limits are respectively:

$$\varepsilon_{c,dc} = 0.004 + 1.4\frac{\rho_v f_{yv} \varepsilon_{su}}{f'_{cc}} \tag{1}$$

$$\varepsilon_{s,dc} = 0.6\varepsilon_{su} \tag{2}$$

where ρ_v and f_{yv} are the volumetric ratio and the yield strength of the transverse reinforcement, respectively, ε_{su} is the monotonic steel strain at maximum strength and f'_{cc} is the compression strength of confined concrete. Eq. (1), obtained by equating the increase in strain energy absorbed by the concrete to the strain capacity of the transversal steel (Mander et al. 1988), represents the occurrence of the fracture of the reinforcement confining the concrete core. This expression is based on pure axial compression of the core concrete, and therefore should be regarded as conservative for flexural loading. Eq.(2), on the other hand, sets the steel strain limit to 60% of the ultimate capacity to account for the possible occurrence of buckling and low cycle fatigue. As stated above, these limits should be regarded as model-specific criteria. For instance, if buckling or low cycle fatigue is explicitly incorporated in the steel model, one can set a higher value for the limit $\varepsilon_{s,dc}$. The occurrence of the strain limits defined by equations (1) and (2) are indicated in most of the figures illustrating the results of the specific case study.

TEST UNIT AND MODELLING APPROACHES

The cantilever wall herein analysed depicts the effective height of a 2/3 scale RC wall representing a typical Swiss building of the 60s. This wall was part of a series of tests on thin RC walls, carried out between September 2013 and May 2014 at the structural engineering laboratory (GIS) of the *École Polytechnique Fédérale de Lausanne* (EPFL). Estimates of the wall responses were required in order to assist with the preparation of the experimental program, giving rise to the current study. The geometry and reinforcement layout of the reference test unit are illustrated in Figure 1.

The wall section length is h=2.7m and its thickness is t=0.12m. It features a small-dimension flange at one of the edges simulating the presence of a perpendicular member. The longitudinal and transversal reinforcement are constituted by 6mm diameter rebars uniformly spaced at 95mm and 130mm respectively. The clear concrete cover is 15mm.

The mechanical features of the reinforcing steel were obtained by carrying out 6 uniaxial tension tests, whose mean stress-strain curve is shown in Figure 2(b). On the other hand, due to the unavailability of mechanical tests on the concrete, a value for the concrete cylinder strength f'_c=37MPa was assumed. In turn, the concrete modulus of elasticity E_c and its tensile strength f'_t were computed according to Priestley et al. (1996) and Lin and Scordelis (1975). Finally, a standard value for the concrete strain ε_c at the maximum stress was used. The reinforcement ratios and the mechanical properties of the employed materials are summarized in Table 2.

In order to assess the relative significance of shear deformations on the structural behaviour, two different shear spans were considered: L_s=2.1m and L_s=8.4m, corresponding to 1 and 4 times the height of the test unit (Figure 1). The resulting shear span ratios L_s/h were 0.78 and 3.12. In both cases a constant axial load N=690kN—equivalent to an axial load ratio of $N/(f'_c \cdot A_g) \cong 5\%$— was applied at the top of the wall, in its centroid.

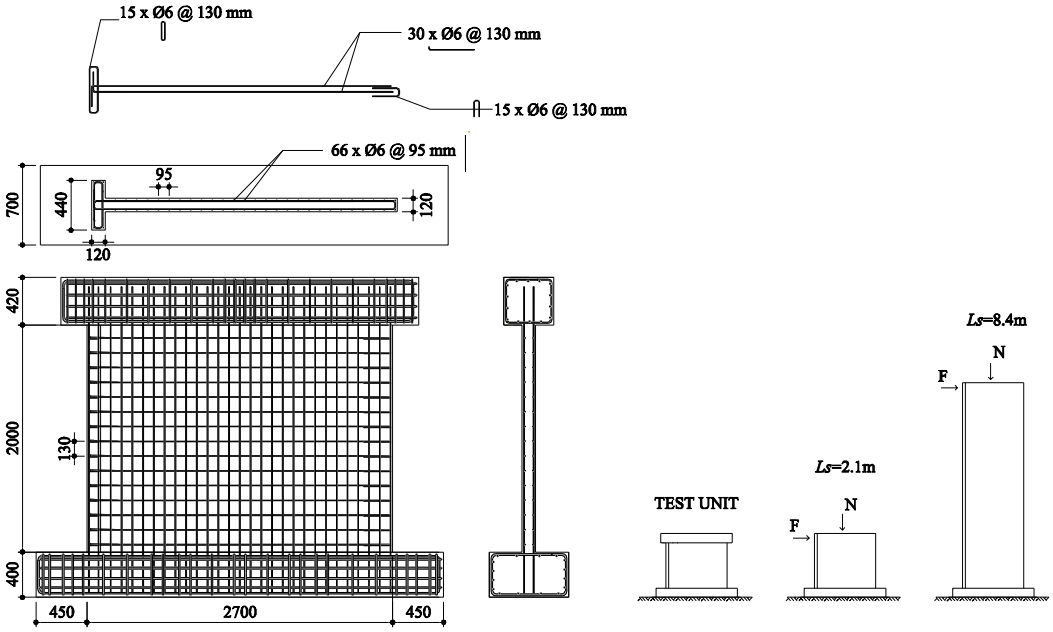

Figure 1: Geometry and reinforcement layout of the test unit, adopted shear spans

Table 2: Mechanical features of the wall: (a) reinforcement ratios, (b) material properties.

REINFORCEMENT RATIOS

	Vertical	Horizontal	Orthogonal
	ρ_v [%]	ρ_h [%]	ρ_{ort} [%]
Web	0.49	0.35	[-]
Flange	0.64	0.19	0.35

MATERIAL PROPERTIES

Concrete	f'_c	ε_c	E_c	f'_t		
	[MPa]	[‰]	[MPa]	[MPa]		
	37	2	28600	2		
Steel	f_y	f_u	E_s	ε_{sy}	ε_{sh}	ε_{su}
	[MPa]	[MPa]	[MPa]	[‰]	[‰]	[‰]
	484	610	210000	2.3	2.3	82

The material stress-strain curves for all the employed models were chosen in order to minimize the discrepancies amongst the distinct approaches. For the concrete, the relationship proposed by Popovics (1973) was used in all cases. The constitutive law for steel, on the other hand, was chosen between the available software models in order to provide the best fit with the available experimental results (Figure 2). Besides the material properties, the main features of each model are described in the following paragraphs. Further details on the specificities of the models, the modelling choices and the materials calibration procedure can be found in Tarquini (2014).

Two plastic hinge models were considered. The first, which does not account for shear deformations, is based on the formulation proposed by Priestley et al. (2007), with the adaptations therein suggested for wall-type structures. The other uses the same formulation for the flexural deformations but also accounts for shear deformation using the approach by Beyer et al. (2011). The damage control strain limits, as specified in the previous section, were used to define the ultimate conditions. The sectional analysis was performed with the open source software OpenSees (OpenSees, 2013)—herein labelled as 'OS'—using a refined layer discretization for cover and core concrete. The properties of confined concrete were determined according to Mander et al. (1988), using a geometrical effectiveness coefficient of confinement C_e=0.5 as recommended by Priestley et al. (2007) for wall-type elements. The obtained values for the confined concrete maximum strength and the corresponding strain were respectively f'_{cc}=41.3MPa and ε_{cc}=3.16‰. Concerning the steel, rebar buckling was not considered in the model.

For the distributed plasticity models (DPMs), three distinct modelling options were considered to simulate the behaviour of the cantilever wall. They corresponded to different beam element formulations (displacement-based and force-based), mesh discretizations, and numerical integration schemes; their features are summarized in Table 3 and shown in Figure 3. The reference fibre element software used to carry out the analysis of the DPMs was OpenSees. However, in order to assess the differences between existing structural analysis packages that build on distinct uniaxial material models, the case of a FB element with 5 IPs was also implemented in the FE software SeismoStruct (SeismoSoft, 2013)—herein labelled as 'SS'—giving rise to the model 'SS-FB-5IP'. None of the DPMs discussed above accounts for shear deformation. Although there are a few scientific proposals to account for it, they are still not widely validated. Furthermore, they are not broadly spread amongst the engineering community nor implemented in commercial structural analysis software.

The detailed finite element (DFE) simulation was carried out with 2D membrane software VecTor2 (Wong et al. 2014), designated as 'V2' in the figures, developed at the University of Toronto and based on the Modified Compression Field Theory (Vecchio and Collins, 1986). The structure is discretized by plane stress rectangles of RC material with smeared reinforcement (see Figure 3). The cover concrete was not modelled because it was shown not to be significant neither at the global nor at the local levels, and the confinement effects were addressed by assigning explicitly the same peak strength and associated strain indicated above for the sectional analyses.

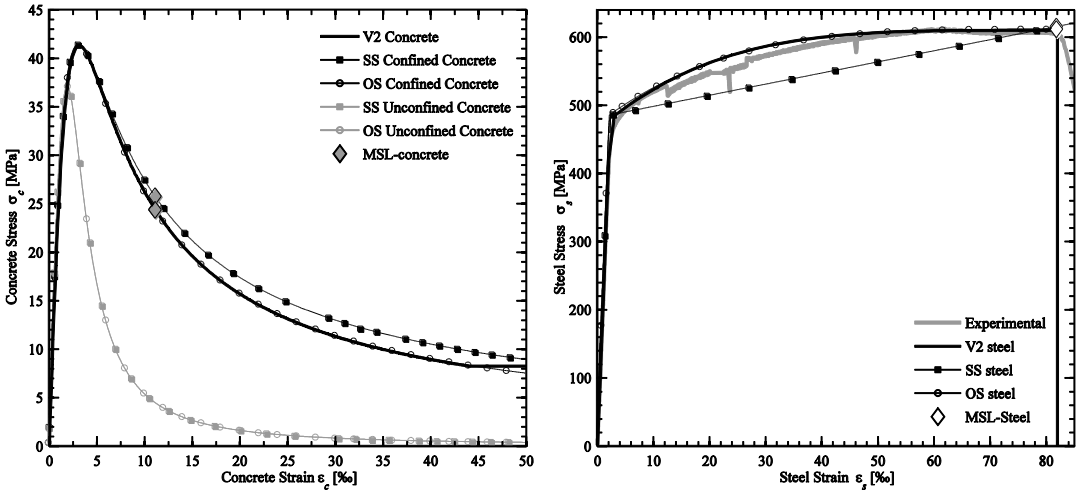

Figure 2: Adopted material constitutive laws: (a) concrete, (b) steel vs experimental.

Table 3: General features of Distributed Plasticity Models (DPMs).

Model	Element type	N° elements	N° Integration Points	Integration Rule
OS-FB-5IP	Force-Based (strict equilibrium)	1	5	Gauss-Lobatto
OS-FB-9IP	Force-Based (strict equilibrium)	1	9	Gauss-Lobatto
OS-DB-PH	Displacement-Based (average equilibrium)	4*	2	Gauss-Legendre

* DB formulation uses displacement interpolation functions: 4 elements are employed to simulate the response of the structural member

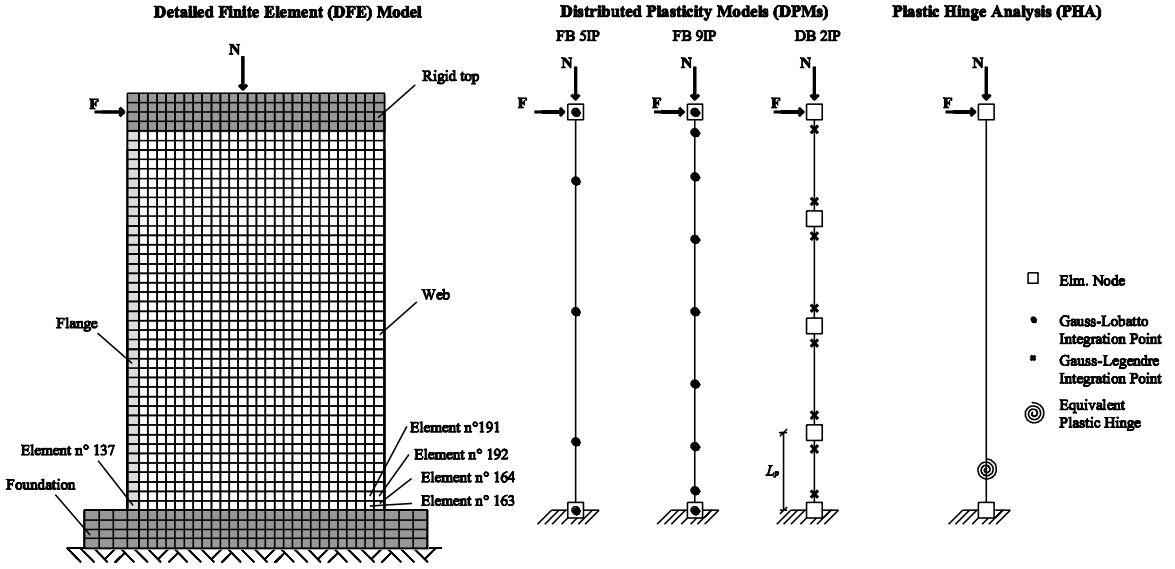

Figure 3: Employed modelling techniques for the simulation of the wall response.

GLOBAL-LEVEL RESPONSE

This section presents and discusses the capacity curves obtained for all the considered models and shear span ratios (Figure 4). On each curve the material strain limit (MSL) and the occurrence of localization (as defined later in the section 'Localization and Numerical Issues') are explicitly indicated. The marker corresponding to the MSL differs whether it is controlled by the attainment of the concrete or steel limit strains. For the case study, they correspond to the attainment of a core concrete strain ε_{cc}=11.2‰ or of a reinforcement strain ε_s=49.2‰ respectively. In regard to the membrane element model, an additional point defining the onset of numerical issues is displayed. In fact, although the capacity curves resulting from DFE models show a smooth behaviour until the end of the analysis, it will be shown (section on *Localization and numerical issues*) that there is a drift beyond which the global results build on an unstable waggling local behaviour.

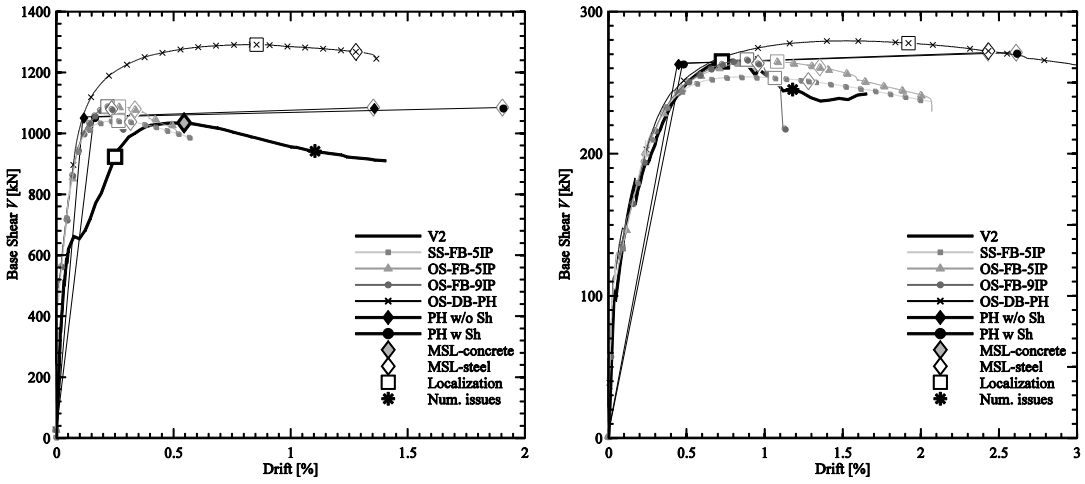

Figure 4: Global-level response comparison: (a) L_s=2.1m; (b) L_s=8.4m.

A few general comments on the figure are due before discussing specifically the results for the two shear span ratios. Firstly, it is noted that the MSLs takes place after the occurrence of numerical localization. In other words, these cases illustrate that performance-based assessments relying solely on the use of material limit strains may be untrustworthy. Secondly, it is apparent that, apart from the DFE models wherein shear can assume a relevant role, the steel MSL is the governing condition. Thirdly, for DPMs with one FB element and five IPs, the differences between the models in OpenSees (OS) and SeismoStruct (SS) can be imparted to the distinct steel constitutive laws; the SS lower-bound stress-strain relation, see Figure 2, reflects into a lower-bound prediction of the associated force-displacement curves. Finally, concerning the OS results, it is observed that the curves for 5 and 9 IPs start diverging in the post-peak branch following the localization onset.

Regarding the results corresponding to the shear span L_s=8.4 m (L_s/h ≈3.1), a good agreement amongst all the proposed models can be observed. The scatter in the predicted lateral capacity of the wall is below 5%, and the stiffness evolution up to the peak strength is consistent. The exception is obviously the PHA models, which—due to the underlying bilinear moment-curvature assumption—exhibit a constant stiffness up to the yield point. For shear span ratios L_s/h >3, shear deformations are expected to play a marginal role (Priestley et al. 2007). That can be confirmed by the similarity of the predictions given by the two PHA models and by the matching of the shear-free DPM responses and the shear-inclusive DFE results. Taking the DFE force-displacement curve as benchmark, the DPMs using force-based (FB) elements appear to give better results than the one employing displacement-based (DB) elements. The latter, although providing good estimates of the wall capacity, seem to grossly overestimate its ductility in comparative terms.

Looking at the case of L_s=2.1m (L_s/h ≈0.78), the clear influence of shear deformations lead to the following observations on the predicted global response of the wall: first off, the DFE capacity curve depicts an increased flexibility in relation to the DPM results; furthermore, the PHA accounting for shear displays a 40% higher ultimate drift than the purely flexural PHA. It is observed however that the application of the latter modelling technique is of little physical meaning. In fact, the assumptions of PHA are no longer applicable to such small shear span ratio, where the plastic hinge length represents more than 30% of the wall height. The figure also shows that the DB approach deviates, as expected, from the remaining models, not only in terms of ductility but also in terms of lateral strength prediction (30% higher than the DFE). Such observation does not come as a surprise since DB formulations provide stiffer and stronger predictions of the actual member response due to the assumption of displacement interpolation functions (de Veubeke, 1965). An objective ('exact') response can only be obtained with a larger number of DB elements, especially where the member demand is higher. This condition is not met in the present case since the base element length corresponds to the equivalent plastic hinge length (as calculated for PHAs). Regarding the comparison between the DFE and the FB approaches, and notwithstanding the acceptable simulation of the member force capacity, the clear influence of shear deformations shows that Euler-Bernoulli beam theory is no longer acceptable.

LOCAL-LEVEL RESPONSE

The local-level response of the wall is now depicted and interpreted for each model and shear span ratio. The vertical strains of both the compressive concrete core and tensile steel are shown in Figure 5(a) and Figure 5(b). The results obtained from the PHAs are not presented since, due to the assumptions of the method, local EDPs (e.g. strains) should not be back-calculated from the results obtained at the global level. Concerning the DPMs, the strains of the extreme fibres are recorded at the section corresponding to the bottom IP. This can be observed in Figure 3, which also depicts the position and number of the elements in the DFE models wherein the vertical strains are tracked. In this latter category of models, several neighbouring elements are monitored for the concrete strains since the response amongst them differs significantly, due to the occurrence of localization. The next section will provide further insights into this numerical problem, which is not evident on the tensile wall side due to the low ratio between the concrete tensile and compressive strengths; therefore, only the steel vertical strains at one element were recorded. Similarly to the global-level response, Figure 5 indicates

the points corresponding to the MSLs, the onset of localization, and the occurrence of numerical issues.

The first fundamental observation from the figure is that the scatter of the strain predictions is significant, at least beyond certain levels of drift. This is not surprising, since strains are highly dependent on the assumptions of each finite element formulation and the deformation mechanisms that they account for. The current numerical example thus shows that the use of strain-based EDPs should always be carefully employed for assessment purposes, and straightforwardly disregarded beyond certain values of drift. In order to define the latter threshold, it is essential to consider the dependability range of the analyses; this, as discussed previously, was defined by the attainment of strain limits, localization onset, or numerical issues, whichever occurred first. Although such range is not a sufficient condition of accuracy, it pinpoints a bound above which finite element simulation becomes progressively (or immediately) nonsensical.

The second relevant overall remark is that the scatter of the predicted (concrete and steel) vertical strains increases for the smaller shear span ratio. As an example, it can be observed that the ratio between the upper and lower-bound concrete strain estimates given by different modelling approaches, at a drift level of 0.2% and L_s=2.1m, is around 5; this ratio can only be found, for L_s=8.4m, at a drift level of approximately 1% (i.e., 5 times larger).

Other insightful comments can be obtained by analysing the strain curves within each plot in more detail. For what concerns concrete, an overall comparison of the DFE curves for the four bottom corner elements show a first evident disagreement: after the localization onset, the strains concentrate in the foundation-contiguous elements no. 163 and 164, while elements no. 191 and 192 show a general unloading trend. The reasons for this behaviour will be analysed in the next section, which will also shed light on the deviation of the FB results with different number of integration points, again after the beginning of localization.

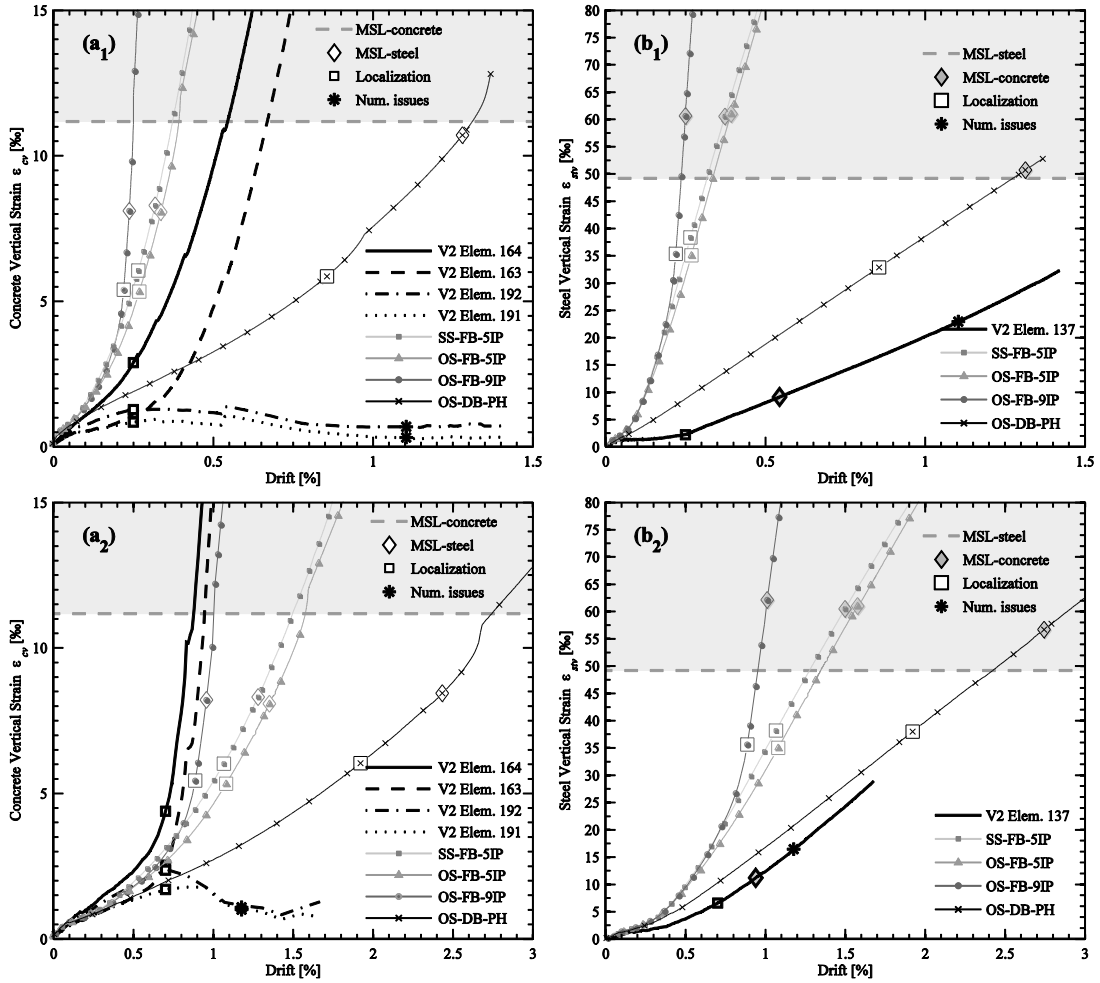

Figure 5: Local-level concrete and steel strains. (a_1) and (b_1): L_s=2.1m; (a_2) and (b_2): L_s=8.4m.

Finally, it is also apparent that the DB model grossly underestimates the vertical strains when compared to the FB approach. This discrepancy, which decreases for the large shear span ratio, is attributable to the DB beam element formulation; namely, the assumed linear curvature profile along each element length, associated with an average verification of equilibrium, creates an artificial restraint in the development of inelastic curvatures amongst the IPs (Calabrese et al. 2010). Regarding the steel strains predicted by the DPMs, analogous observations can be made; it is however noted that, for all the considered shear span ratios, the prediction given by the DFE model defines the lower-bound (see next section).

LOCALIZATION AND NUMERICAL ISSUES

The present section starts by defining the limits of response objectivity applicable both to DPMs and DFE models. Beyond this threshold, the appearance of localization issues entails mesh-dependent results. As pointed out by Bazant (1976), this phenomenon is directly related to particular computational problems occurring with materials described by softening constitutive laws. Such descending branch of the stress-strain relation leads to mathematical difficulties as the boundary value problem becomes ill-posed and the response is no longer unique.

Starting with the DPMs (FB-5IP, FB-9IP, DB), the moment-curvature curves of the sections located in the proximity of the wall base, for the case of L_s=8.4m, are displayed in Figure 6. Each curve shows ten markers indicating equal intervals of drift until a maximum value δ_{max} corresponding to a drop of 10% of the wall capacity. The flexural capacity of the section for the applied axial load is also reported by a horizontal grey dashed line.

As observable in Figure 6 for FB-5IP, after the peak of the moment-curvature response in the base section (attained for $\phi \approx 12 km^{-1}$, 6th marker, plot a_1), the deformations start concentrating therein whereas the section above begins to unload (plot a_2). The same behaviour can be noticed for FB-9IP model—plots (b_1) and (b_2)—with the notable difference that the curvature concentration in the base section progresses at a much faster rate: For the FB element with 5 IPs, an increase in base curvature from 12 to 32 km^{-1} leads to an increase in drift of $0.4\delta_{max}$ (plot a_1). For the FB with 9 IPs, the same increase in curvature leads only to an increase in drift of $0.2\delta_{max}$ (plot b_1). This is due to the different integration weights of the base section where the deformations concentrate (0.028 for FB-9IP and 0.1 for FB-5IP, out of a total element integration weight of 2). A very distinguishable localization pattern occurs for DB formulations, wherein curvatures concentrate simultaneously in both sections of the base element: as shown in plot (c_3), it is the bottom section of the second element above the base that starts unloading. Furthermore it is noticeable that the maximum moments from the sectional results of the base element, plots (c_1) and (c_2), differ from the maximum flexural capacity of the section for the applied axial load. This discrepancy is due to the fact that DB formulations do not strictly verify equilibrium and hence the axial force along the element equals only on average the load applied externally, i.e., the axial force is different for the two IPs.

The occurrence of localization in DFE analyses is shown in Figure 7(a) for L_s=8.4m. It shows the vertical stress-strain curves of the 4 elements located at the compressed wall corner (Figure 3). The σ_v-ε_v curves are plotted up to a drift level of 0.8%, which roughly corresponds to the peak of the global force-displacement response. Again, markers on each curve represent equally spaced drift intervals.

The interpretation of the results indicates that above a certain drift level the strains concentrate in the foundation-contiguous elements (no. 163 and 164), while the elements of the row above (no. 191 and 192) start to unload. In this study, the drift level at the onset of localization for DFE models has been identified by the occurrence of the first negative post-yield slope of the vertical compressive stress-strain relation, amongst all the elements of the mesh. This was considered as a cautious but reliable indicator of the beginning of mesh-dependent results. It is however noted that in DFE models the existence of stress and strain gradients (e.g. in walls) typically minimize the relevance of localization, when compared to members in approximately uniform compression (e.g. concrete cylinders, axially loaded column).

Figure 7(b) shows the same vertical stress-strain curves of Figure 7(a), for elements no. 163 and 164, however extended until the end of the analysis (drift level of 1.7%). The purpose of these plots is to show, for strains above approximately 5.5%, the occurrence of a waggling behaviour of the stress-

strain curves which is indicative of unidentified numerical issues. The latter are common (e.g. convergence problems), and to a certain extent inevitable, in structural analysis software; however they can often be corrected, alleviated, or even eliminated for specific combinations of input parameters, material or element models, convergence criteria, global solution methods, etc. Such combinations are difficult to define *a priori*, hence in general the user should be aware of the likely occurrence these numerical problems, which render the computational output untrustworthy; therefore, the authors decided to explicitly include the identification of this phenomenon in the analyses, defining its manifestation under the broad designation of 'numerical issue'. It is highlighted that the local-level waggling behaviour of specific elements (such as the one depicted in Figure 7(b)) does not necessarily reflect at the global-level response (Figure 4); the importance of carrying out a multi-level assessment of the structure is therefore, and once again, strongly recommended.

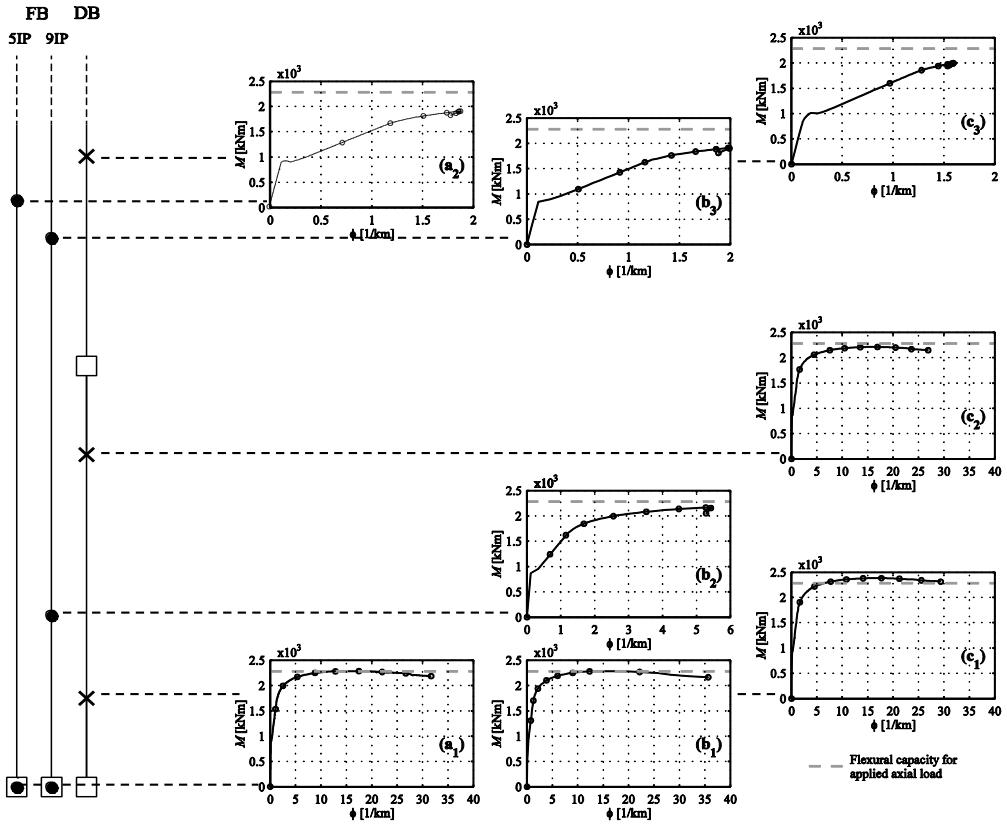

Figure 6: Numerical localization in DPMs (FB and DB), near the wall base.

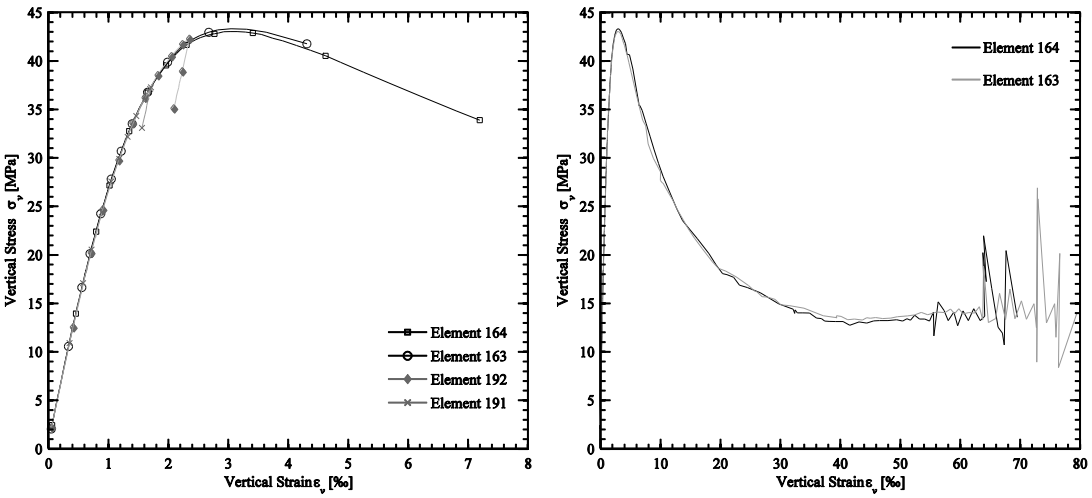

Figure 7: DFE models: (a)Numerical localization; (b)Numerical issues due to analysis instability.

SHEAR DEFORMATION

The effect of shear deformations, which are only accounted for in DFE models, is addressed in the following paragraphs (the simple PHA with shear does not manage to provide an insight on the member behaviour). The ratio of shear-to-flexural deformation (Δ_s/Δ_f) for the different shear span ratios increases for decreasing shear span ratios: it is of the order of 10% for L_S=8.4m, and higher than 50% for L_S=2.1m (Tarquini, 2014).

The vertical and shear strains profiles of the wall base section corresponding to three different drift levels are shown in Figure 8. They were chosen as representative of (i) a close-to-elastic phase, (ii) the beginning of the inelastic response, and (iii) the attainment of the wall lateral force capacity (designated as 'peak drift').

Concerning the vertical strains it is possible to notice how the approximately linear distribution for 10% of the 'peak drift' progressively evolves to a nonlinear distribution at larger demands. This remark holds independently of the chosen shear span ratio and points out the limitation of the plane-section-remaining-plane hypothesis assumed for DPMs.

The shear strain profiles, besides depending on the considered drift level, seem to be affected by the shear span ratio as well; their absolute value increases with the drift level and decreases with the shear span. Furthermore, it can be observed that, for L_S=8.4m, the shear strain distribution remains approximately constant along the entire section of the wall independently of the imposed drift. Such fact suggests that, for elements behaving predominantly in flexure, the constant shear strain hypothesis—as adopted by Timoshenko beam theory—seems to be reasonable. The previous rationale, on the other hand, does not appear valid for the small shear span ratio (even for nearly elastic response), since the shear strain profile cannot be assimilated to a constant function. Eventually, for higher values of drift, shear strains tend to clearly concentrate on the compressed section side.

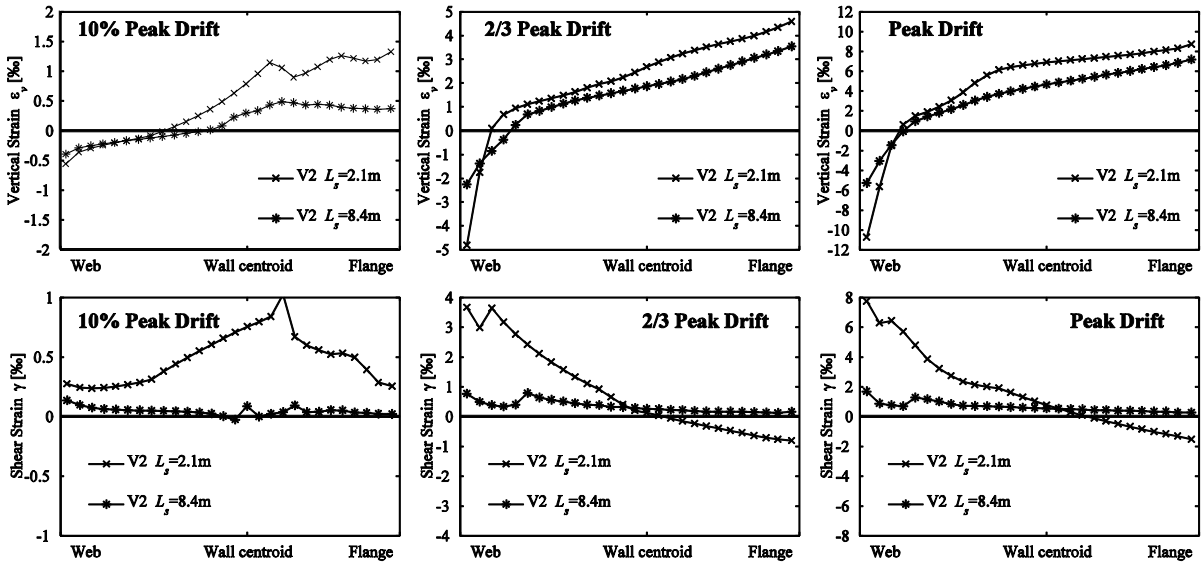

Figure 8: Vertical and shear strain profiles at the wall base.

CONCLUSIONS

The inelastic behaviour of RC walls can at present be simulated by a variety of modelling techniques. In the present work, results obtained from plastic hinge analyses (PHAs), distributed plasticity models (DPMs) and detailed finite element (DFE) simulations are investigated and compared. Each approach can be seen as a composition of levels of analysis that are interconnected through a number of specific shared variables. The need to carry out a multi-level interpretation of the output in order to evaluate

the dependability of a structural assessment procedure is the first conclusion of this study. It is also shown that, despite the noticeable advances on numerical simulation methods over the past decades, the employed modelling techniques provide a scatter of predictions that increases dramatically from the global to the local level. This feature must be carefully taken into account as local EDPs are increasingly used in performance-based design and assessment. Additionally, this work indicates the importance of estimating the range of the results that can be considered as reliable, which should take into account three distinct aspects: material strain limits, localization and other numerical issues. Finally, it was shown that for small shear span ratios the disagreement between the outcomes of distinct simulation methods at the local level is much more pronounced than at the global level.

REFERENCES

ASCE 7-02. (2002). *Minimum Design Loads for Buildings and Other Structures*. *ASCE Standard*.

ATC-3-06. (1978). *Tentative Provisions for the Development of Seismic Regulations for Buildings*. *Applied Technology Council*. California.

Bazant, Z. P. (1976). Instability, ductility and size effect in strain-softening concrete. *Journal of the Engineering Mechanics Division*, *102*(2), 331–344.

Berry, M. P., Lehman, D. E., & Lowes, L. N. (2008). Lumped-plasticity models for performance simulation of bridge columns. *ACI Structural Journal*, *105*(3), 270–279.

Beyer, K., Dazio, A., & Priestley, M. J. N. (2011). Shear deformations of slender reinforced concrete walls under seismic loading. *ACI Structural Journal*, *108*(2), 167–177.

Bozorgnia, Y., & Bertero, V. V. (2004). *Earthquake Engineering - From Engineering Seismology to Performance-Based Engineering*. *CRC Press* (p. 941).

Calabrese, A., Almeida, J. P., & Pinho, R. (2010). Numerical issues in distributed inelasticity modeling of RC frame elements for seismic analysis. *Journal of Earthquake Engineering*, *14*(S1), 38–68.

De Veubeke, B. F. (1965). Displacement and equilibrium models in the finite element method. In *Stress Analysis* (O.C. Zienk., Vol. 52, pp. 145–197). John Wiley & Sons. doi:10.1002/nme.339

EN1998-1. (2002). *Eurocode 8: Design of Structures for Earthquake Resistance. Part 1: General Rules, Seismic Actions and Rules for Buildings. Doc CEN/TC250/SC8/N306. European Committee for Standardization*.

EN1998-3. (2005). *Eurocode 8: Design of Structures for Earthquake Resistance. Part 3: Assessment and Retrofitting of Buildings. Doc CEN/TC250/SC8/N306. European Committee for Standardization*.

FEMA. (2012). *FEMA P-58-1: Seismic Performance Assessment of Buildings, Volume 1 - Methodology*. *Applied Technology Council, Federal Emergency Management Agency* (Vol. 1).

Lin, C.-S., & Scordelis, A. C. (1975). Nonlinear analysis of RC shells of general form. *Journal of the Structural Division*, *101*(3), 523–538.

Mackie, K., & Stojadinovic, B. (2001). Seismic demands for performance-based design of bridges. In *PEER Annual Meeting*.

Mander, J. B., Priestley, M. J. N., & Park, R. (1988). Theoretical Stress-Strain Model for Confined Concrete. *Journal of Structural Engineering*, *114*(8), 1804–1826.

OpenSees. (2013). Open System for Earthquake Engineering Simulation - Version 2.4.3.

Popovics, S. (1973). A numerical approach to the complete stress-strain curve of concrete. *Cement and Concrete Research*, *3*(5), 583–599. doi:10.1016/0008-8846(73)90096-3

Priestley, M. J. N., Calvi, G. M., & Kowalsky, M. J. (2007). *Displacement-based Seismic Design of Structures*. *IUSS Press* (p. 721).

Priestley, M. J. N., Seible, F., & Calvi, G. M. (1996). *Seismic Design and Retrofit of Bridges*. *John Wiley & Sons* (p. 686).

SEAOC. (1959). *Recommended Lateral Force Requirements and Commentary*. *Seismology Committee, Structural Engineers Association of California* (First.).

SEAOC. (1980). *Recommended Lateral Force Requirements and Commentary*. *Seismology Committee, Structural Engineers Association of California* (Fourth.).

SeismoSoft. (2013). SeismoStruct - A Computer Program for Static and Dynamic Nonlinear Analysis of Framed Structures.

Tarquini, D. (2014). *Modelling Approaches for Inelastic Behaviour of RC Walls: Multi-level Assessment and Dependability of Results*. IUSS - Istituto Universitario di Studi Superiori, Pavia.

Vecchio, F. J., & Collins, M. P. (1986). The modified compression-field theory for reinforced concrete elements subjected to shear. *ACI Journal*, *83*(2), 219–231.

Wong, P. S., Vecchio, F. J., & Trommels, H. (2014). VecTor2 - Nonlinear Analysis of Two-Dimensional Reinforced Concrete Membrane Structures.